Journal of Physics:
Conference Series

PAPER • **OPEN ACCESS**

Magnetic flux rope: What is it?

To cite this article: Qiang Hu 2023 *J. Phys.: Conf. Ser.* **2544** 012002

Magnetic flux rope: What is it?

Qiang Hu

320 Sparkman Drive, CSPAR and Department of Space Science, The University of Alabama in Huntsville, Huntsville, AL 35805, USA

E-mail: qiang.hu@uah.edu

Abstract. Magnetic flux rope, a type of magnetic field structure in space plasmas, has been studied for decades through both observational and theoretical means. We provide a brief report on our recent modeling study of its magnetic field configuration based on in-situ spacecraft measurements, focusing on those made for large-scale flux ropes in the interplanetary space. We illustrate the complexity in its field-line topology by presenting two event studies employing a unique analysis method. In particular, we demonstrate the feasibility and challenges for the approach to use two or more in-situ spacecraft datasets. We discuss the implications of our results and offer some thoughts on further advancing the investigation of the nature of the magnetic flux rope.

1. Introduction

Magnetic flux rope is generally believed to form the core structure of a coronal mass ejection (CME) on the Sun upon its eruption. The evidence supporting this view becomes particularly strong when a CME is crossed in-situ by an observing spacecraft at larger heliocentric distances. Such crossings enable direct sampling of the plasma medium and the magnetic field embodied within a CME, thus the so-called interplanetary CME (ICME), yielding time-series measurements across a propagating ICME complex at a single point or along a single line. These observational signatures include but are not limited to, 1) enhanced magnetic field magnitude relative to the ambient solar wind, 2) smooth rotation in one or two field components, and 3) depressed proton β value (the ratio between the proton pressure and the magnetic pressure). A structure spanning an interval with all three aforementioned signatures present is classified as a magnetic cloud (MC) and is generally believed to possess a magnetic flux rope configuration [1, 2, 3]. Other ICME structures possessing two, one, or arguably none of those three signatures can still possess a magnetic flux rope configuration, especially when the correspondences to the source CME eruptions are certain. This generally calls for well coordinated observational analysis combining the modern remote-sensing observations of the Sun and adequate analysis methods taking into account the realistic complexity in the magnetic field topology of (I)CMEs (see, e.g., [4]).

Conceptually MCs are thought to possess well-organized magnetic field configuration since their first identification from in-situ spacecraft data. The most common model based on in-situ data assumes a cylindrical one-dimensional (1D) geometry [5, 1]. This type of configuration exhibits a field-line topology similar to a slinky and this general view has not evolved much over the past few decades. In this configuration, field lines are winding around a central axis on distinct surfaces with regularly shaped cross sections, i.e., mostly concentric circles or ellipses.

One significant extension to this type of models is a complete two-dimensional (2D) model based on the Grad-Shafranov (GS) equation, which yields a 2D arbitrary cross section directly derived from the spacecraft measurements along its path across the structure [6, 7, 8, 9]. One step further in the latest development is a quasi-three dimensional (3D) model that adds 3D spatial variations to a magnetic flux rope configuration [10, 11, 12]. It has been applied to a number of event studies, especially in connection with the solar source CME magnetic field topology that is characterized by more general 3D field-line configurations [13, 14, 4].

The question of what defines a magnetic flux rope remains, despite decades of observations and research. The exception, in our view, or one way to address this question is through multiple observations including remote-sensing imagery and numerical modeling of solar source regions of flares/CMEs. For example, a field-line twist number can be quantified and used to identify a flux rope structure by specifying a threshold value [15]. However it remains challenging for applying a unified approach to perform such numerical simulations in order to obtain reliable results [16]. For relevant modeling and analysis of in-situ measurements, it is equally challenging to achieve a high level of certainty. In this report, we do not intend to address this question in a definitive manner, but to demonstrate the necessity of going beyond the traditional 1D or 2D view of a magnetic flux rope configuration. Then one may achieve the goal of defining a magnetic flux rope in the most general as well as the simplest terms.

This report is organized as follows. Section 2 describes briefly the quasi-3D model for a magnetic flux rope and the optimal fitting approach. The set of analytic formulations is given. Section 3 presents two selected case studies by applying the quasi-3D model for the purpose of demonstrating the feasibility of the approach and the complexity in the magnetic flux rope configurations that may not be addressed by other models. Section 4 summarizes the case study results and discusses our view toward and the outlook for the analysis of magnetic flux ropes in space plasmas.

2. A quasi-3D model for magnetic clouds

It is highly desirable to move forward with a 3D model for the in-situ analysis of MCs to account for the reality of complex magnetic field topology clearly seen in countless studies of their solar source regions. One of such models has been developed recently by applying a set of formulations well known in fusion science [17] for a linear force-free magnetic field configuration. Namely, for the magnetic induction, $\mathbf{B}$, satisfying $\nabla \times \mathbf{B} = \mu \mathbf{B}$ with $\mu = Const$, the three components of the magnetic field can be written explicitly in a cylindrical coordinate system [17], (r, θ, z),

$$\frac{B_z(\mathbf{r})}{B_{z0}} = J_0(\mu r) + C J_1(lr)\cos(\theta + kz), \tag{1}$$

$$\frac{B_\theta(\mathbf{r})}{B_{z0}} = J_1(\mu r) - \frac{C}{l}\left[\mu J_1'(lr) + \frac{k}{lr} J_1(lr)\right]\cos(\theta + kz), \tag{2}$$

$$\frac{B_r(\mathbf{r})}{B_{z0}} = -\frac{C}{l}\left[k J_1'(lr) + \frac{\mu}{lr} J_1(lr)\right]\sin(\theta + kz). \tag{3}$$

Here the solution, dubbed Freidberg solution (FS), obviously has 3D spatial variations with the r dependence governed by the Bessel functions of the first kind. The constant parameters are C, k, and μ (with $l = \sqrt{\mu^2 - k^2}$), representing the amplitude of the non-axisymmetric part, a wavenumber along the z dimension, and the linear force-free constant, respectively. The magnetic field and spatial variables are normalized by a constant B_{z0} and a length scale a [10, 11], respectively.

A standard χ^2 minimization procedure following [18], as given below,

$$\chi^2 = \frac{1}{\mathtt{dof}} \sum_{\nu=X,Y,Z} \sum_{i=1}^{N} \frac{(b_{\nu i} - B_{\nu i})^2}{\sigma_i^2}, \tag{4}$$

is devised to obtain a set of optimal parameters that determines a solution consistent with the spacecraft measurements along one or more paths across the solution domain [10, 11]. We name this approach the FS model fitting method. Here the reduced χ^2 value is evaluated along one single path or multiple separate spacecraft paths (for the latter, see [12]). Differences between the measured magnetic field **b** and the FS model output are evaluated component-wise, subject to the uncertainty estimates σ_i and the degree-of-freedom (`dof`), complying with the χ^2 statistics [18]. Detailed descriptions of the optimization procedures are given in [11].

One word of caution is that when performing this kind of optimization/minimization analysis, a proper evaluation of the uncertainties, σ_i, in the denominator of the formula inside the summation sign of equation (4) is critical for an objective assessment of the goodness-of-fit. If such uncertainties were arbitrarily enlarged (for example, by substituting the total magnetic field magnitude for this quantity), the principle of this analysis approach would be violated, rendering meaningless results.

Table 1. Locations of Solar Orbiter and Wind spacecraft on 30 May 2020, 00:00 UT in the Carrington coordinates (courtesy of Solar-MACH [19], `https://da.gd/gzoINr`).

Position	Solar Orbiter	Wind
R (AU)	0.56	1.0
longitude (°)	282	252
latitude (°)	4.1	-0.9

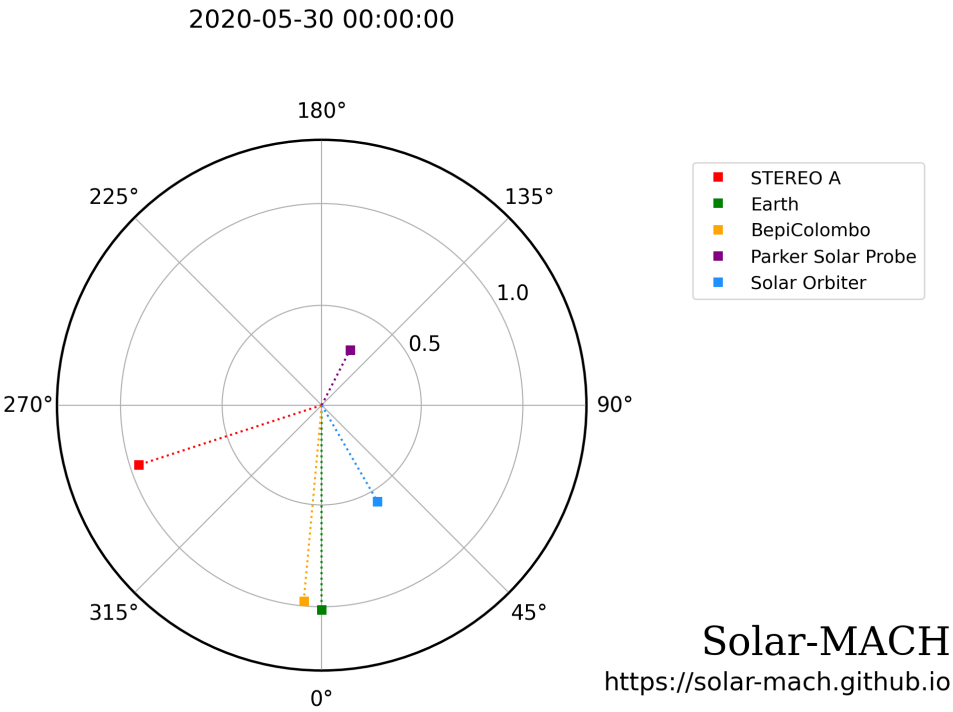

Figure 1. The Solar Orbiter and Wind spacecraft (Earth) locations on 30 May 2020 on the Sun's equatorial plane (see the legend and Table 1 for the corresponding coordinates).

3. Case studies: complexity in magnetic flux rope configurations

We present in this section two event studies to illustrate the complexity in the magnetic flux rope configurations by applying the FS model fitting approach to in-situ spacecraft data. By presenting these results, we hope to stimulate interest and the realization of the need to expand or reformulate the "conventional" perception about a magnetic flux rope.

3.1. Event 1: ICME on 30 May 2020

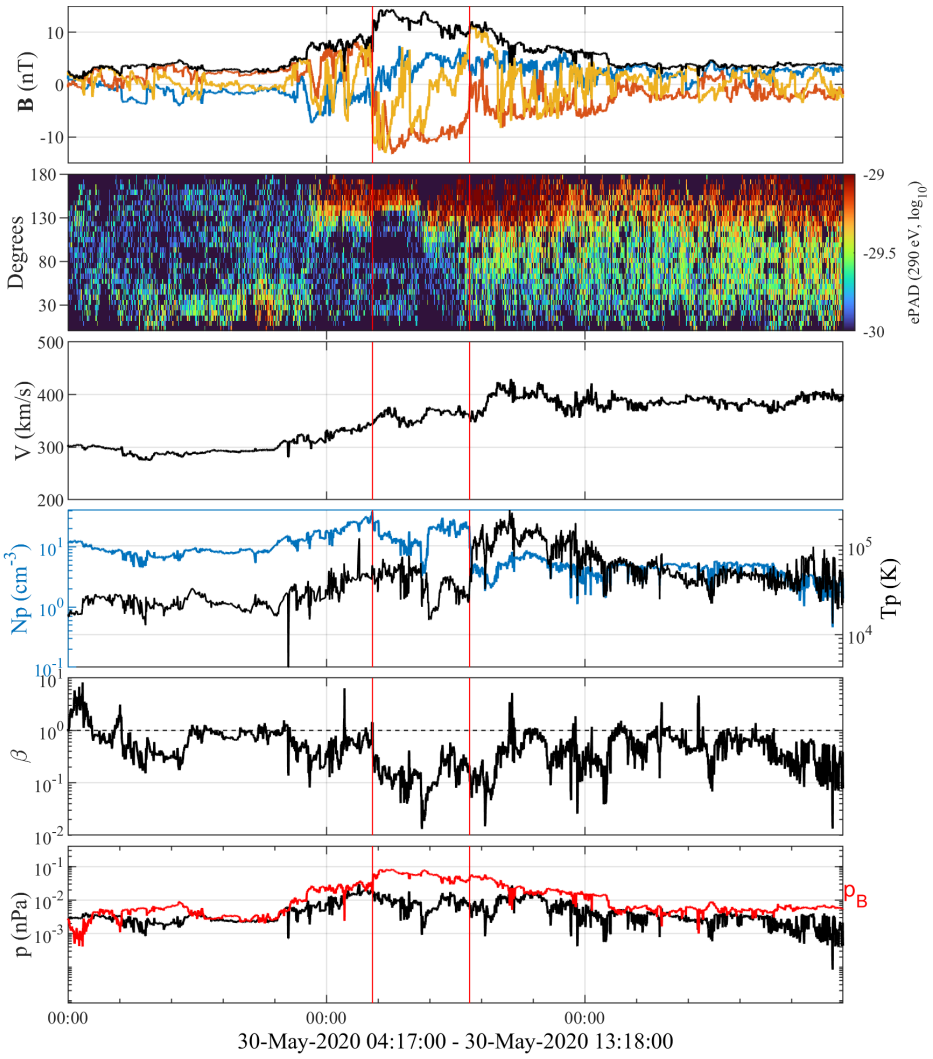

Figure 2. Time series from Wind spacecraft in-situ measurements for the time period, May 29 - June 1, 2020. From the top to bottom panels are: magnetic field components in GSE-X (blue), Y (red), and Z (gold) coordinates, and the magnitude (black), the electron pitch angle distributions (ePADs) with color scales given by the color bar to the right, the solar wind speed, the proton density and temperature, the proton β, and the proton and magnetic (red) pressure. The interval chosen for analysis is marked by the vertical red lines and is denoted beneath the last panel in UT.

Event 1 occurred during a time period with multi-spacecraft encounters in addition to the in-situ measurements by the Wind spacecraft at Earth. In particular the newly launched Solar

Orbiter (SO; [20]) was believed to have crossed the same ICME complex [21] at a heliocentric distance $R \approx 0.56$ AU with a longitudinal separation of 30° from Earth (see Table 1 for the spacecraft locations information). Figure 1 shows the locations of a number of spacecraft on the solar equatorial plane at the time. Three spacecraft, BepiColombo (BC), Wind and SO had intercepted the same ICME at different times due to their different locations as shown. The in-situ measurements from BC are not available to us and we can only obtain the SO magnetic field measurements for the time period we have examined. Figure 2 shows the usual set of time-series measurements from Wind spacecraft, including the ePADs data from the Solar Wind Experiment (SWE) instrument. The two vertical lines mark the interval selected for the FS model fitting method described in Section 2. The three signatures mentioned in Section 1 for an MC are present during this interval, supporting the following analysis by the FS model fitting. In addition, the ePADs show relatively prominent signatures of streaming electrons in the anti-field direction ($\sim 180°$ PA), which can also be confirmed by the similar data (not shown) by the 3D Plasma (3DP) instrument. Figure 3 shows the corresponding magnetic field measurements at SO obtained about 1 day earlier. At SO, the signatures of a magnetic flux rope structure are more prominent with stronger magnetic field magnitude and a more pronounced rotation in the B_N component during the interval between DOY 149.8 and DOY 150.4.

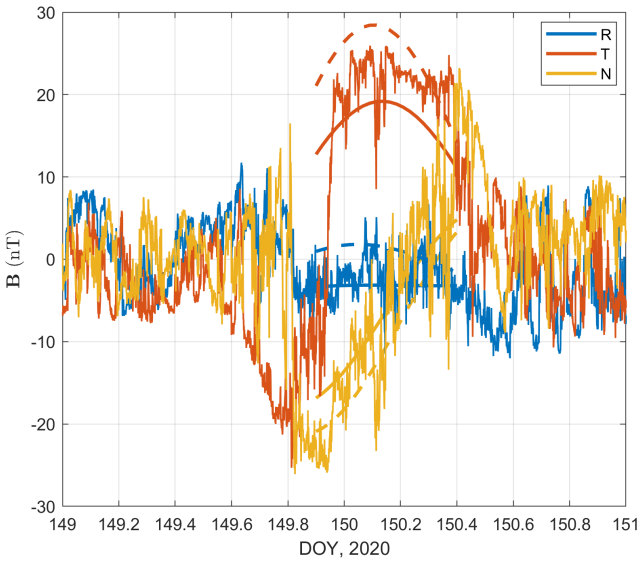

Figure 3. The SO magnetic field components in the spacecraft centered Radial (R), Tangential (T) and Normal (N) coordinates for the time period 28 - 30 May 2020 (day of year, DOY 149 - 151, 2020). The smooth curves are the FS model output discussed in Section 3.1.

We have demonstrated in recent studies [4, 12, 13] the necessity of employing more than one spacecraft dataset in the FS model fitting. This event study represents our latest effort and an extreme case in terms of the widest separation distance between the two spacecraft. Based on the assumption that both Wind and SO spacecraft encountered the same ICME structure (see also [21] for detailed discussions), we carry out the two-spacecraft dataset optimization approach [12] by employing both Wind and SO spacecraft data shown in Figures 2 and 3 for the FS model fitting. Figure 4 shows the optimal fitting result: left panel shows the fitting result of the FS model output and measured magnetic field components along the Wind spacecraft path across the analysis interval with the minimum reduced $\chi^2 = 1.86$; right panel shows one cross section

of the FS model solution with the two spacecraft paths projected in this view down the z axis. It shows a configuration with one dominant positive polarity region enclosed by the boundary (dotted magenta line) where $B_z = 0$. The model output along the SO spacecraft path is denoted in Figure 3 by the smooth solid curves for the three components. The corresponding dashed curves are the estimates by assuming a radial evolution of the axial magnetic field B_z based on the consideration of the conservation of the axial magnetic flux content Φ_z [13].

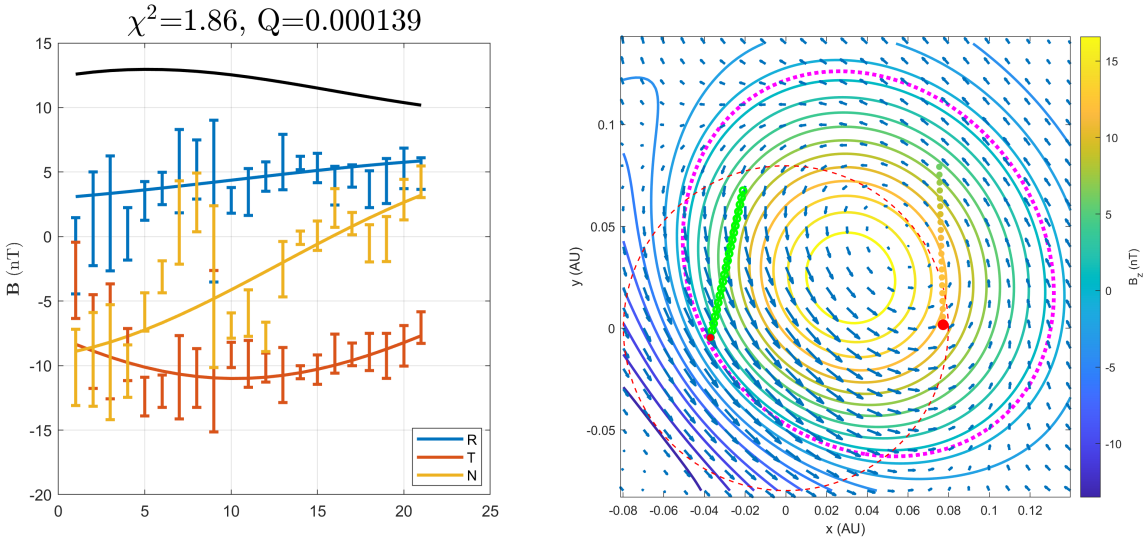

Figure 4. The FS model fitting result to the combined Wind and SO spacecraft datasets. Left panel: the optimal model fitted (smooth curves) and measured (errorbars) magnetic field components along the Wind spacecraft path; black curve is the fitted field magnitude. Right panel: the cross section of the magnetic field configuration at $z = 0$ from the fitted FS model; the contours are the axial field component B_z with scales indicated by the color bar, the arrows are the transverse field vectors, and the Wind and SO spacecraft paths are denoted by the points to the right, color coded by the B_z component, and the green points to the left, respectively; the dotted magenta line marks the boundary of the positive polarity region where $B_z = 0$.

Figure 5 puts the whole FS model solution domain in a view that better reveals the flux rope configuration from the encountering Wind spacecraft's perspective in space. The main flux bundle (orange lines) is winding mostly in the East-West direction and the SO spacecraft has a path across the middle while the Wind spacecraft path appears to cross the edge to the South. As a check for this type of analysis using two sets of in-situ spacecraft data, one can further examine the correlation between the FS model output and the actual measured magnetic field components along the secondary spacecraft's path, i.e., SO's path in this case. Such a comparison is shown in Figure 6. The overall correlation coefficient between the two sets of magnetic field components is $cc = 0.94$.

One caveat, however, is that a simple timing analysis based on an unknown but assumed constant average traveling speed between SO and Wind fails to yield a reasonable time delay consistent with the observations at the two spacecraft as shown above. If the whole configuration demonstrated in Figure 5 is believed to be reasonable based on the current analysis, then a highly variable kinematic evolution between the two spacecraft has to occur, which has yet to be verified based on current available observations. The processes unaccounted for between two or more observing probes pose significant challenges for this type of analysis, especially when

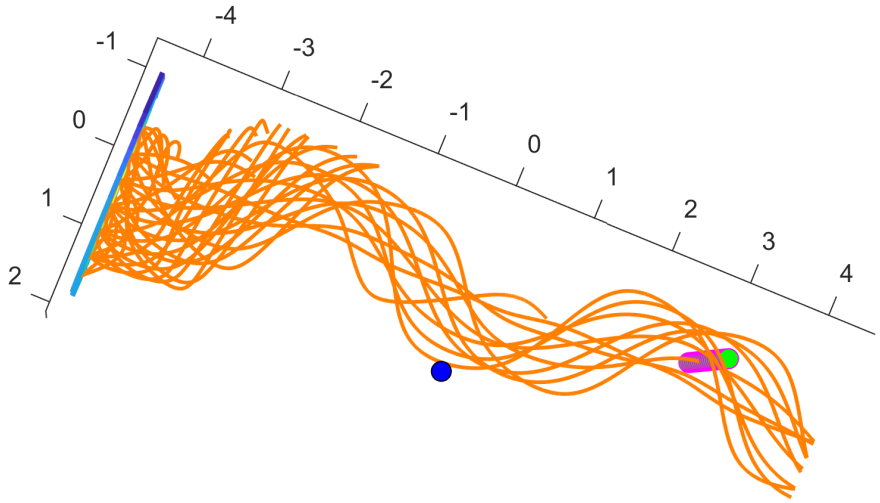

Figure 5. The 3D view of the FS model fitted field-line configuration along the Wind spacecraft path (blue dot) toward the Sun. The East-West direction is horizontal and North is upward. The orange lines are the field lines originating from the cross section shown to the East. The SO spacecraft path (green dots) across the same structure is shown to the West. The tickmark labels are normalized by a length scale $a = 0.080$ AU.

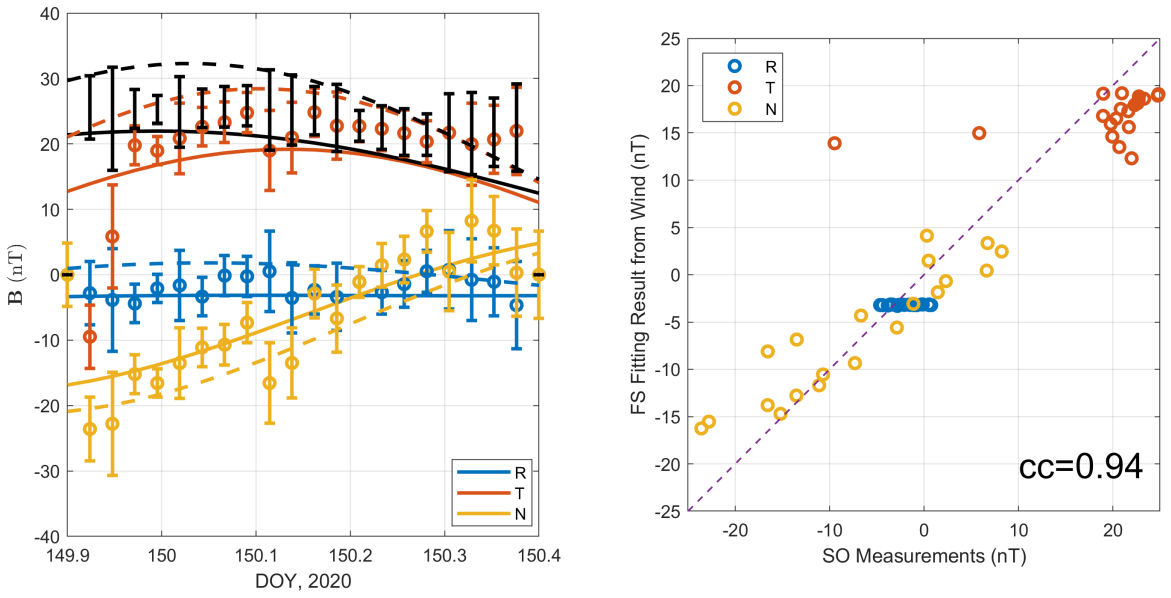

Figure 6. The correlation between the measured magnetic field components (circles with errorbars) and the FS model fitting results (smooth curves) along the SO spacecraft path based on the 3D configuration shown in Figures 4 and 5. See Section 3.1 for details.

the separations are relatively large as they are for this case.

3.2. Event 2: ICME on 9 March 2012

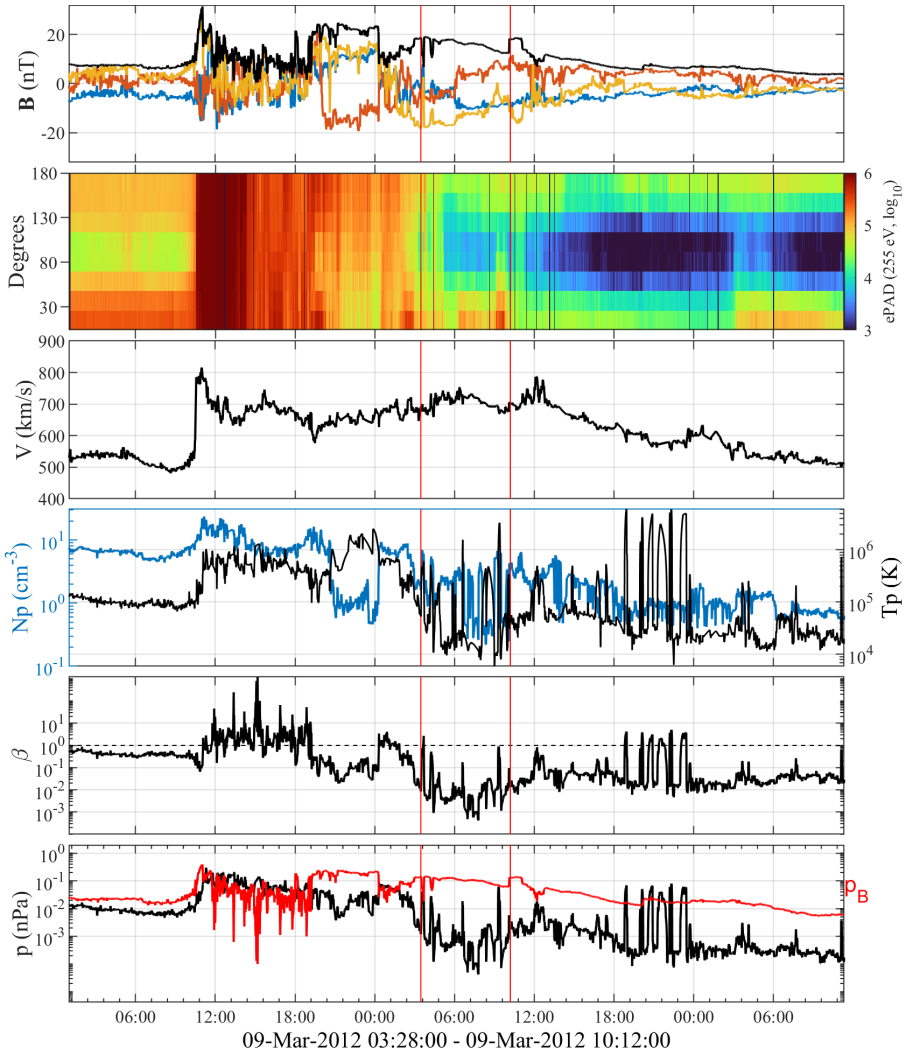

Figure 7. Time series from the Wind spacecraft in-situ measurements for the time period March 8 - 11, 2012. Format is the same as Figure 2. The second panel shows the ePADs from the Wind/3DP instrument.

To further illustrate the level of complexity as revealed from in-situ modeling of ICME magnetic flux ropes, we present one more analysis of the ICME event on 9 March 2012. Figure 7 shows again the time-series measurements from the Wind spacecraft. An ICME complex is seen preceded by a shock wave with a turbulent sheath region. The analysis interval with relatively strong and smooth magnetic field falls behind, characterized by significantly reduced proton β value (in the order of 0.01) and relatively steady solar wind speed. The ePADs data from Wind/3DP (the corresponding SWE data have significant gaps) show a slight hint of bi-directional electrons streaming mainly along the 0° and 180° PA directions during the interval. Figure 8 shows the usual output for the optimal FS model fitting by using the Wind spacecraft data from the selected interval. The result is acceptable as indicated by the minimum reduced $\chi^2 = 1.26$ and the corresponding goodness-of-fit parameter Q [18, 11]. The cross section perpendicular to $\hat{\mathbf{z}}$ shows two major polarities with opposite signs of the B_z component. The

spacecraft path appears to be embedded entirely inside the flux bundle of the negative polarity. This is confirmed by a rendering of the 3D field-line configuration in Figure 9 with a viewpoint from the ecliptic north onto the ecliptic plane. The overall field-line configuration exhibits two flux bundles winding around each other that are spiraling mainly along the Sun-Earth direction and nearly lying on the ecliptic plane, but are oppositely directed. The Wind spacecraft path crosses the flux bundle in cyan color in the left panel of Figure 9, where the cyan field lines are all pointing downward (anti-sunward) in this view. The orange color field lines, on the other hand, are all pointing upward. In the right panel of Figure 9, only selected field lines intercepting the Wind spacecraft path and a pair of field lines originating near the location of the maximum B_z in the positive polarity region are highlighted in blue and red colors, respectively. A number of blue field lines disperses widely with the footpoints spreading irregularly on the bottom cross section as shown, although the overall appearance may still resemble a "tight" spiral shape as commonly perceived.

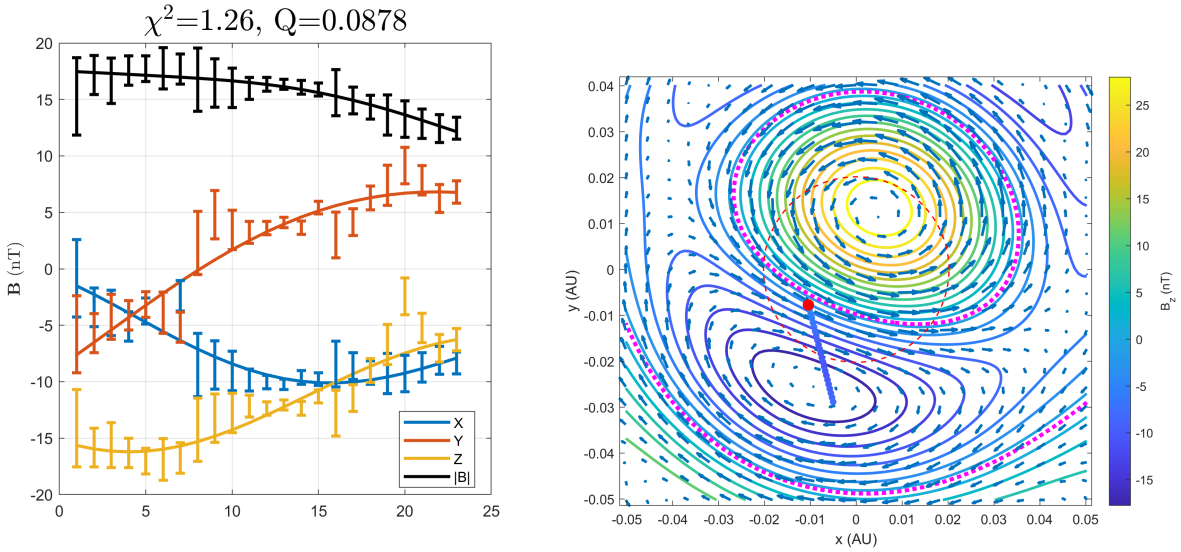

Figure 8. The optimal fitting result for Event 2 on 9 March 2012 by using the Wind spacecraft in-situ measurements. Format is the same as Figure 4.

One more aspect as demonstrated in Figure 9 is that the Wind spacecraft path misses the main body of the flux bundle illustrated by the orange field lines rooted in the positive polarity region on the cross-section plane. Whether this flux bundle is part of one entire ICME flux system has yet to be determined by examining the solar source region eruption(s) of the corresponding flare(s) and/or CME(s).

4. Summary and discussion: "food for thought"

In summary, we have presented two case studies of ICME magnetic flux ropes by using the quasi-3D FS model fitting approach to the in-situ spacecraft measurements. Their main parameters are summarized in Table 2. They show a typical range of magnitudes of the axial magnetic flux contents Φ_z (in the order of tera Wb, TWb) similar to prior results obtained by using the 2D GS reconstruction method [22]. For Event 2, the axial magnetic flux contents for both the positive (+) and negative (-) polarity regions are given and they are close in magnitudes. However the 3D spatial features such as the clear variation along the axial (z) dimension are distinct from other 1D or 2D models (see also [4, 14, 10]). Therefore one needs to keep an open mind as

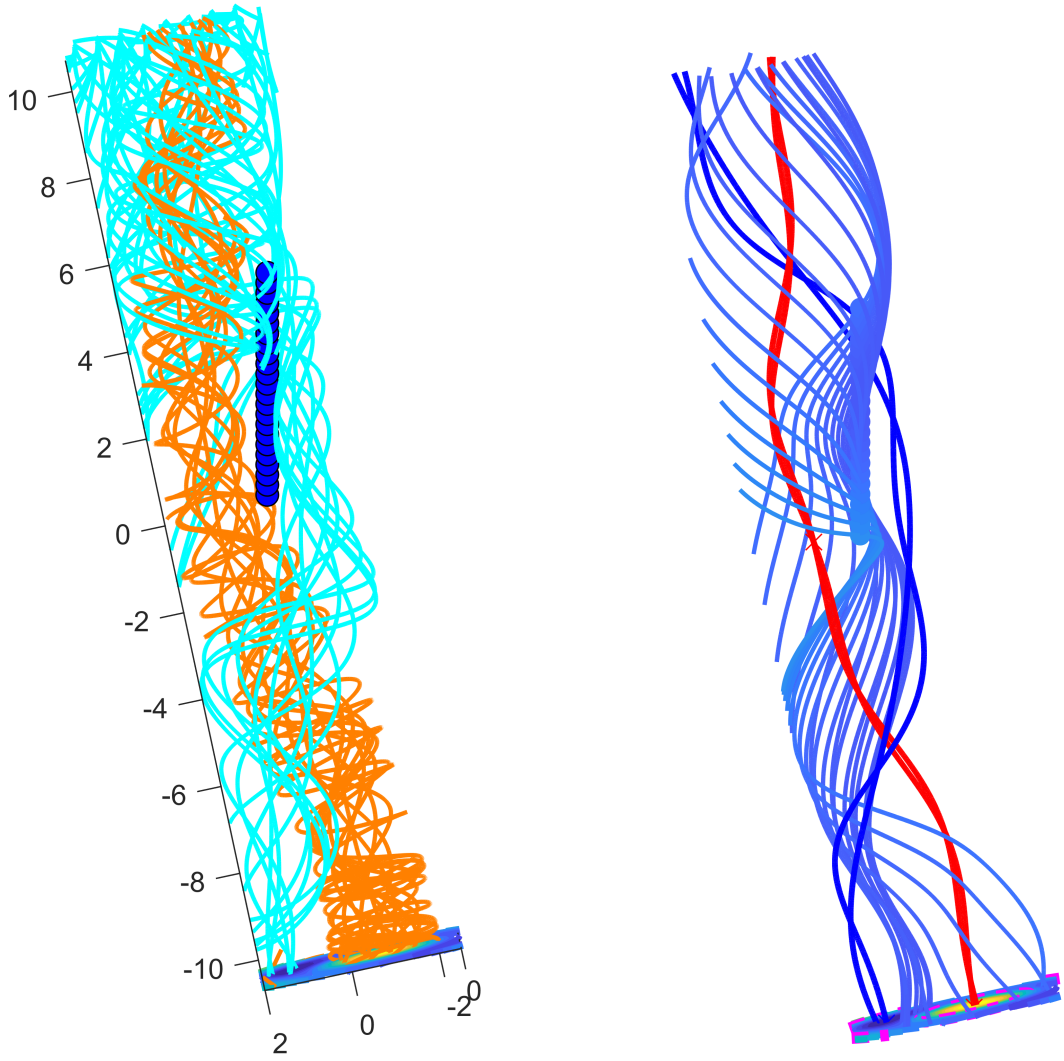

Figure 9. Left panel: the 3D view of the field-line configuration of Event 2 down from the ecliptic North (Sun is in the upward direction). The orange and cyan lines are field lines rooted on the positive and negative polarity regions on the cross-section plane in the bottom. The blue dots form the Wind spacecraft path for this analysis interval. Tickmark labels are normalized by a length scale $a = 0.020$ AU. Right panel: the same view as the left panel but with only selected field lines intercepting the Wind spacecraft path color coded by the B_z component (all negative), while the red lines are rooted near the maximum B_z of the positive polarity region.

far as a definition of a "magnetic flux rope" is concerned. Our current view is that from the perspective of terminology, the historic term "magnetic clouds" may be used interchangeably with "magnetic flux ropes". A universal definition of a magnetic flux rope can be sought from solar observations and analysis, especially concerning the CME magnetic field topology. Then the question naturally becomes whether a magnetic flux rope always constitutes an essential part of the structure of a CME. The answer may be positive if one adopts a broader definition of a magnetic flux rope, e.g., that of a "ribbon-like" field-line topology [4, 12].

Table 2. Summary of primary FS model parameters for the two events.

Parameters	$\hat{\mathbf{z}}$ (GSE)	CB_{z0} (nT)	ka	μa	Φ_z (TWb)
Event 1	[0.022, -0.92, -0.38]	22	1.4	2.4	+4.5
Event 2	[0.99, 0.11, 0.086]	-38	-0.29	1.8	-1.0/+0.83

One may add to the title of this report the additional question, "What is it good for?". As widely recognized, the importance and prevalence of a magnetic flux rope structure to CMEs are well established. It is generally believed that flux rope formation prior to and during flare/CME eruptions plays a critical role in the associated dynamic evolution processes. The CME flux rope configurations have been well manifested in in-situ observations of ICMEs, which occupy the far-right end portion of the scale-size distribution of magnetic flux ropes more extensively identified over a wide range of scale sizes [23]. The so-called small to intermediate-scale magnetic flux ropes are found to be much more prevalent in the interplanetary space and their scale sizes exhibit a continuous power-law distribution [23]. They are intrinsically related to the magnetohydrodynamic turbulence and play active roles in particle energization and heating of plasmas, based on recent studies [24, 25], a few also included in this volume. For those topics beyond the scope of this report, we refer interested readers to those works, and in particular, to an online database of small-scale magnetic flux ropes at `http://fluxrope.info`, for event lists from multiple spacecraft missions and the relevant references. Last but not the least, the Earth's magnetospheric environment or more generally the planetary environments provide another space plasma regime for exploring the nature of magnetic flux ropes.

Acknowledgments
We thank Dr. Gary Zank (Co-I of the SO mission) and Dr. Lingling Zhao for providing the SO magnetic field data for this study. The author also benefited from the on-going collaboration with Prof. Jiong Qiu at the Montana State University. We acknowledge support from NASA grants 80NSSC19K0276, 80NSSC21K0003, 80NSSC21K1671, and NSF grants AGS-1954503, AGS-2020703, and AGS-2050340. The Wind spacecraft data are downloaded from the NASA CDAWeb and OMNIWeb Plus.

References

[1] Burlaga L F, Klein L, Sheeley N R J, Michels D J, Howard R A, Koomen M J, Schwenn R and Rosenbauer H 1982 *Geophys. Res. Lett.* **9** 1317–1320
[2] Burlaga L F 1988 *Journal of Geophysical Research: Space Physics* **93** 7217–7224 URL `https://agupubs.onlinelibrary.wiley.com/doi/abs/10.1029/JA093iA07p07217`
[3] Lepping R P, Burlaga L F and Jones J A 1990 *J. Geophys. Res.* **95** 11957–11965
[4] Hu Q, Zhu C, He W, Qiu J, Jian L K and Prasad A 2022 *Astrophys. J.* **934** 50 (*Preprint* `2204.03457`)
[5] Lundquist S 1950 *Ark. Fys.* **2** 361
[6] Hu Q 2017 *Sci. China Earth Sciences* **60** 1466–1494
[7] Hau L N and Sonnerup B U Ö 1999 *J. Geophys. Res.* **104** 6899–6918
[8] Hu Q and Sonnerup B U Ö 2001 *Geophys. Res. Lett.* **28** 467–470
[9] Hu Q and Sonnerup B U Ö 2002 *J. Geophys. Res. (Space Physics)* **107** 1142
[10] Hu Q, He W, Qiu J, Vourlidas A and Zhu C 2021 *Geo. R. Letts.* **48** e90630 (*Preprint* `2010.11889`)
[11] Hu Q 2021 *Solar Phys.* **296** 101 (*Preprint* `2104.09352`)
[12] Hu Q, He W and Chen Y 2022 *Frontiers in Physics* **10** 960315 (*Preprint* `2206.01247`)
[13] Hu Q, He W, Zhao L and Lu E 2021 *Frontiers in Physics* **9** 407 ISSN 2296-424X URL `https://www.frontiersin.org/article/10.3389/fphy.2021.706056`

[14] He W, Hu Q, Jiang C, Qiu J and Prasad A 2022 *Astrophys. J.* **934** 103 (*Preprint* 2201.03149)
[15] Liu R, Kliem B, Titov V S, Chen J, Wang Y, Wang H, Liu C, Xu Y and Wiegelmann T 2016 *The Astrophysical Journal* **818** 148 URL https://doi.org/10.3847/0004-637x/818/2/148
[16] Jiang C, Feng X, Guo Y and Hu Q 2022 *The Innovation* **3** 100236 ISSN 2666-6758 URL https://www.sciencedirect.com/science/article/pii/S2666675822000327
[17] Freidberg J P 2014 *Ideal MHD* (Cambridge, UK: Cambridge University Press) pp 546–547
[18] Press W H, Teukolsky S A, Vetterling W T and Flannery B P 2007 *Numerical Recipes in C++ : The Art of Scientific Computing* (New York: 778, Cambridge Univ. Press)
[19] Gieseler J, Dresing N, Palmroos C, von Forstner J L F, Price D J, Vainio R, Kouloumvakos A, Rodríguez-García L, Trotta D, Génot V, Masson A, Roth M and Veronig A 2022 Solar-mach: An open-source tool to analyze solar magnetic connection configurations URL https://arxiv.org/abs/2210.00819
[20] Müller, D, St Cyr, O C, Zouganelis, I, Gilbert, H R, Marsden, R, Nieves-Chinchilla, T, Antonucci, E, Auchère, F, Berghmans, D, Horbury, T S, Howard, R A, Krucker, S, Maksimovic, M, Owen, C J, Rochus, P, Rodriguez-Pacheco, J, Romoli, M, Solanki, S K, Bruno, R, Carlsson, M, Fludra, A, Harra, L, Hassler, D M, Livi, S, Louarn, P, Peter, H, Schühle, U, Teriaca, L, del Toro Iniesta, J C, Wimmer-Schweingruber, R F, Marsch, E, Velli, M, De Groof, A, Walsh, A and Williams, D 2020 *A&A* **642** A1 URL https://doi.org/10.1051/0004-6361/202038467
[21] Weiss A J, Möstl C, Davies E E, Amerstorfer T, Bauer M, Hinterreiter J, Reiss M A, Bailey R L, Horbury T S, O'Brien H, Evans V, Angelini V, Heyner D, Richter I, Auster H U, Magnes W, Fischer D and Baumjohann W 2021 *Astron. Astrophys.* **656** A13 (*Preprint* 2103.16187)
[22] Hu Q, Qiu J, Dasgupta B, Khare A and Webb G M 2014 *Astrophys. J.* **793** 53 (*Preprint* 1408.1470)
[23] Hu Q, Zheng J, Chen Y, le Roux J and Zhao L 2018 *The Astrophysical Journal Supplement Series* **239** 12 URL https://dx.doi.org/10.3847/1538-4365/aae57d
[24] le Roux J A and Zank G P 2021 *Astrophys. J.* **913** 84
[25] Zank G P, Nakanotani M, Zhao L L, Du S, Adhikari L, Che H and le Roux J A 2021 *Astrophys. J.* **913** 127